Inorganic Chemistry
Article

*Inorg. Chem.* **2010**, *49*, 10283–10290 **10283**
DOI: 10.1021/ic100694w

# Theoretical Investigations on the Chemical Bonding, Electronic Structure, And Optical Properties of the Metal−Organic Framework MOF-5

**Li-Ming Yang,[†] Ponniah Vajeeston,[‡] Ponniah Ravindran,[‡] Helmer Fjellvåg,[‡] and Mats Tilset*[,†]**

[†]*Center of Theoretical and Computational Chemistry and* [‡]*Center for Materials Science and Nanotechnology, Department of Chemistry, University of Oslo, P.O. Box 1033 Blindern, N-0315 Oslo, Norway*

Received April 12, 2010

The chemical bonding, electronic structure, and optical properties of metal−organic framework-5 (MOF-5) were systematically investigated using ab initio density functional calculations. The unit cell volume and atomic positions were optimized with the Perdew−Burke−Ernzerhof (PBE) functional leading to a good agreement between the experimental and the theoretical equilibrium structural parameters. The calculated bulk modulus indicates that MOF-5 is a soft material. The estimated band gap from a density of state (DOS) calculation for MOF-5 is about 3.4 eV, indicating a nonmetallic character. As MOFs are considered as potential materials for photocatalysts, active components in hybrid solar cells, and electroluminescence cells, the optical properties of this material were investigated. The detailed analysis of chemical bonding in MOF-5 reveals the nature of the Zn−O, O−C, H−C, and C−C bonds, that is, Zn−O having mainly ionic interaction whereas O−C, H−C, and C−C exhibit mainly covalent interactions. The findings in this paper may contribute to a comprehensive understanding about this kind of material and shed insight into the synthesis and application of novel and stable MOFs.

## I. Introduction

Metal−organic frameworks (MOFs) constitute a new generation of porous crystals.[1] They can be described as crystalline hybrid inorganic/organic solids with structures which are composed of clusters of a few metal atoms held together in a three-dimensional structure by organic linkers. This class of compounds has the remarkable advantage of combining both organic and inorganic fragments as part of the same structure. The remarkable crystallinity of MOF structures defines pores and cavities on the nanometric scale. The possibility for guest molecules to enter the internal voids of MOFs, frequently of high volume, causes these materials in many respects to resemble the behavior of zeolites. However, MOFs are attractive not only because of the structural diversity that they provide but also because of their remarkable physicochemical properties. Currently, MOFs are considered as important materials of academic interest and with possible industrial applications within catalysis, petrochemistry, gas adsorption and storage (e.g., $H_2$, $CH_4$, $CO_2$, etc.), selective separation, sensing, molecular recognition, and so on.[1,2]

The diversity in composition along with different modes of preparation and handling has led to MOFs with a wide range of properties suitable for the various applications, and new MOFs are reported at an ever increasing pace.[3] However, the appearance of fundamentally new, stable inorganic building blocks within MOFs is less common. Within the huge MOF family of structures, the most well-known example is probably MOF-5 (IRMOF-1),[4] which is the first member of a series of isoreticular MOFs (IRMOFs)[5−7] with oxide-centered $Zn_4O$ tetrahedra as nodes linked by organic molecules. The prototypical MOF-5 has a highly symmetric cubic structure, is relatively simple to synthesize, and up to now, it has been subject to a plethora of investigations from experimental as well as theoretical perspectives.[8] Investigations have also been conducted to tailor the electronic properties of MOF-5.[9,10] Other efforts addressed the electrostatic potential and charge density for MOF-5[11] to gain additional insight

*To whom correspondence should be addressed. E-mail: mats.tilset@kjemi.uio.no. Fax: +47 22855441.

(1) *Chem. Soc. Rev.* **2009**, *38*, (5): Special issue on MOFs.
(2) Czaja, A. U.; Trukhan, N.; Müller, U. *Chem. Soc. Rev.* **2009**, *38*, 1284–1293.
(3) Long, J. R.; Yaghi, O. M. *Chem. Soc. Rev.* **2009**, *38*, 1213–1214.
(4) Li, H.; Eddaoudi, M.; O'Keeffe, M.; Yaghi, O. M. *Nature* **1999**, *402*, 276–279.
(5) Li, H.; Eddaoudi, M.; Groy, T. L.; Yaghi, O. M. *J. Am. Chem. Soc.* **1998**, *120*, 8571–8572.
(6) Eddaoudi, M.; Moler, D. B.; Li, H.; Chen, B.; Reineke, T. M.; O'Keeffe, M.; Yaghi, O. M. *Acc. Chem. Res.* **2001**, *34*, 319–330.
(7) Ockwig, N. W.; Delgado-Friedrichs, O.; O'Keeffe, M.; Yaghi, O. M. *Acc. Chem. Res.* **2005**, *38*, 176–182.
(8) Keskin, S.; Liu, J.; Rankin, R. B.; Johnson, J. K.; Sholl, D. S. *Ind. Eng. Chem. Res.* **2009**, *48*, 2355–2371.
(9) Choi, J. H.; Choi, Y. J.; Lee, J. W.; Shin, W. H.; Kang, J. K. *Phys. Chem. Chem. Phys.* **2009**, *11*, 628–631.
(10) Fuentes-Cabrera, M.; Nicholson, D. M.; Sumpter, B. G.; Widom, M. *J. Chem. Phys.* **2005**, *123*, 124713/1–12471/5.
(11) Civalleri, B.; Napoli, F.; Noël, Y.; Roetti, C.; Dovesi, R. *CrystEngComm* **2006**, *8*, 364–371.


Published on Web 10/20/2010

into the interaction of $H_2$ with MOF-5. Mechanical properties of MOF-5, including bulk moduli and elastic constants, have been studied.[12,13] Very recently, MOF-5 has attracted additional attention for possible use as quantum dot,[14] photocatalyst,[15] and semiconductor[16] materials.

An improved and comprehensive understanding about the many interesting properties of MOF-5 in various aspects is still desired, which will optimize MOF-5 for potential industrial applications. Especially, the following issues still need to be addressed:

(1) To the best of our knowledge, there is no systematic and detailed investigation on the character of chemical bonding in MOF-5. The bonding interaction between the constituents is important to understand the chemical and physical properties of a system, including structure, stability, and physicochemical properties of MOF-5, and will help to improve its applications in gas absorption, catalysis, sensing, and molecular recognition. Additionally, it will guide the understanding of other MOFs.

(2) Numerous contributions have focused on the spectroscopic properties of MOF-5. These include XRD,[4,17−21] IR,[22,23] UV−vis,[21] NMR,[19,21,24] INS,[25,26] NPD,[27] DRIS,[28] SCND,[29] Raman,[14] EDX,[30] THz TDS,[20] DRIFT,[15] XANES,[31] XAS,[21] TEM,[21] EXAFS,[21] photoluminescence,[16] and time-resolved diffuse reflectance spectra.[16] Particularly, recent experiments have demonstrated that IRMOFs can be used as efficient photocatalysts with a tunable band gap.[15] Furthermore, it has been experimentally demonstrated that ZnO is the origin of the quantum dot behavior in MOF-5.[14] The presence of inorganic semiconductor quantum entities (such as dots or wires) in close contact with organic molecules make the optical properties of MOFs particularly interesting. However, to our knowledge, there is no detailed theoretical report on the optical properties of MOF-5 available.

In the present work, we have performed a computational study on the crystal structure, stability, electronic structure, chemical bonding, mechanical, and optical properties of MOF-5 using density functional theory (DFT) calculations with the GGA-PBE functional implemented in the VASP code.[32,33] The optical properties of MOF-5 were calculated using the CASTEP module[34] of the Material Studio 4.2 program.[35] A central feature of the paper is the detailed investigation of the chemical bonding and optical properties for MOF-5, which we believe will provide valuable insight into this novel class of material for their use as reverse shape-selective photocatalysts, as photoactive materials for photovoltaic cells, and as components for electroluminescence devices.

## II. Computational Details

The Vienna ab initio simulation package (VASP)[32,33] has been used for the total energy calculations to study the structural stability and to establish equilibrium structural parameters. The generalized gradient approximation (GGA)[36−38] includes the effects of local gradients in the charge density for each point in the materials and generally gives better equilibrium structural parameters than the local density approximation (LDA). Hence, the GGA functional was used for all calculations. The projector-augmented-wave (PAW)[33,39] Perdew, Burke, and Ernzerhof (PBE)[38] pseudopotentials were used to describe the ion-electron interactions. A criterion of 0.01 meV $atom^{-1}$ was placed on the self-consistent convergence of the total energy, and all calculations were made with plane-wave cutoff of 500 eV, which guarantees that absolute energies are converged to within a few meV/f.u. This has been tested to be accurate and reliable for the MOF-5 system. Brillouin-zone integration was performed with a Gaussian broadening of 0.2 eV during all relaxations. Since the input structure is taken from the experimental data, which should provide a good initial structure, a quasi-Newton (variable metric) algorithm was used to relax the ions into their instantaneous ground state. The forces and the stress tensor were used to determine the search directions for finding the equilibrium positions (the total energy was not

(12) Bahr, D. F.; Reid, J. A.; Mook, W. M.; Bauer, C. A.; Stumpf, R.; Skulan, A. J.; Moody, N. R.; Simmons, B. A.; Shindel, M. M.; Allendorf, M. D. *Phys. Rev. B: Condens. Matter* **2007**, *76*, 184106/1–184106/7.
(13) Samanta, A.; Furuta, T.; Li, J. *J. Chem. Phys.* **2006**, *125*, 084714/1–084714/8.
(14) Bordiga, S.; Lamberti, C.; Ricchiardi, G.; Regli, L.; Bonino, F.; Damin, A.; Lillerud, K.-P.; Bjørgen, M.; Zecchina, A. *Chem. Commun.* **2004**, 2300–2301.
(15) Gascon, J.; Hernández-Alonso, M. D.; Almeida, A. R.; van Klink, G. P. M.; Kapteijn, F.; Mul, G. *ChemSusChem* **2008**, *1*, 981–983.
(16) Alvaro, M.; Carbonell, E.; Ferrer, B.; Llabrés i Xamena, F. X.; Garcia, H. *Chem.—Eur. J.* **2007**, *13*, 5106–5112.
(17) Kaye, S. S.; Dailly, A.; Yaghi, O. M.; Long, J. R. *J. Am. Chem. Soc.* **2007**, *129*, 14176–14177.
(18) Choi, J.-S.; Son, W.-J.; Kim, J.; Ahn, W.-S. *Microporous Mesoporous Mater.* **2008**, *116*, 727–731.
(19) Schröder, F.; Henke, S.; Zhang, X.; Fischer, R. A. *Eur. J. Inorg. Chem.* **2009**, 3131–3140.
(20) Schröck, K.; Schröder, F.; Heyden, M.; Fischer, R. A.; Havenith, M. *Phys. Chem. Chem. Phys.* **2008**, *10*, 4732–4739.
(21) Müller, M.; Hermes, S.; Kähler, K.; van den Berg, M. W. E.; Muhler, M.; Fischer, R. A. *Chem. Mater.* **2008**, *20*, 4576–4587.
(22) Bordiga, S.; Vitillo, J. G.; Ricchiardi, G.; Regli, L.; Cocina, D.; Zecchina, A.; Arstad, B.; Bjørgen, M.; Hafizovic, J.; Lillerud, K. P. *J. Phys. Chem. B* **2005**, *109*, 18237–18242.
(23) Vitillo, J. G.; Regli, L.; Chavan, S.; Ricchiardi, G.; Spoto, G.; Dietzel, P. D. C.; Bordiga, S.; Zecchina, A. *J. Am. Chem. Soc.* **2008**, *130*, 8386–8396.
(24) Stallmach, F.; Gröger, S.; Künzel, V.; Kärger, J.; Yaghi, O. M.; Hesse, M.; Müller, U. *Angew. Chem., Int. Ed.* **2006**, *45*, 2123–2126.
(25) Rowsell, J. L. C.; Eckert, J.; Yaghi, O. M. *J. Am. Chem. Soc.* **2005**, *127*, 14904–14910.
(26) Zhou, W.; Yildirim, T. *Phys. Rev. B: Condens. Matter* **2006**, *74*, 180301/1–180301/4.
(27) Yildirim, T.; Hartman, M. R. *Phys. Rev. Lett.* **2005**, *95*, 215504/1–215504/4.
(28) FitzGerald, S. A.; Allen, K.; Landerman, P.; Hopkins, J.; Matters, J.; Myers, R.; Rowsell, J. L. C. *Phys. Rev. B: Condens. Matter* **2008**, *77*, 224301/1–224301/9.
(29) Spencer, E. C.; Howard, J. A. K.; McIntyre, G. J.; Rowsell, J. L. C.; Yaghi, O. M. *Chem. Commun.* **2006**, 278–280.
(30) Petit, C.; Bandosz, T. J. *Adv. Mater.* **2009**, *21*, 4753–4757.
(31) Mattesini, M.; Soler, J. M.; Ynduráin, F. *Phys. Rev. B* **2006**, *73*, 094111/1–094111/8.
(32) Kresse, G.; Furthmüller, J. *Comput. Mater. Sci.* **1996**, *6*, 15–50.
(33) Kresse, G.; Joubert, D. *Phys. Rev. B: Condens. Matter* **1999**, *59*, 1758–1775.
(34) Segall, M. D.; Lindan, P. J. D.; Probert, M. J.; Pickard, C. J.; Hasnip, P. J.; Clark, S. J.; Payne, M. C. *J. Phys.: Condens. Matter* **2002**, *14*, 2717–2744.
(35) *Materials Studio*, ver. 4.2; Accelrys: San Diego, CA, 2007.
(36) Perdew, J. P. In *Electronic Structure of Solids*; Ziesche, P., Eschrig, H., Eds.; Akademie Verlag: Berlin, 1991; pp 11−20.
(37) Perdew, J. P.; Burke, K.; Wang, Y. *Phys. Rev. B: Condens. Matter* **1996**, *54*, 16533–16539.
(38) Perdew, J. P.; Burke, K.; Ernzerhof, M. *Phys. Rev. Lett.* **1996**, *77*, 3865–3868.
(39) Blöchl, P. E. *Phys. Rev. B: Condens. Matter* **1994**, *50*, 17953–17979.

taken into account). This algorithm is very fast and efficient close to local minima. Forces on the ions were calculated using the Hellmann−Feynman theorem as the partial derivatives of the free electronic energy with respect to the atomic positions, and adjusted using the Harris−Foulkes correction to the forces. The atoms were relaxed toward equilibrium until the Hellmann−Feynman forces were less than $10^{-3}$ eV Å$^{-1}$.

Because we are dealing with a large system (106 atoms per primitive cell), the Γ-point alone was sufficient for sampling the Brillouin zone during geometry optimization. But to arrive at an accurate band structure and density of state (DOS), the DOS calculation was performed on the fully optimized structure with the **k**-point grid of $3 \times 3 \times 3$ using the Monkhorst−Pack scheme. Furthermore, the DOS was calculated in a fine energy grid (1801 points) because of the narrow band features so as to visualize DOS correctly.

To gauge the bond strength and character of bonding, we have analyzed bond overlap population (BOP) values estimated on the basis of the Mulliken population as implemented in the CASTEP code.[34] To understand the chemical bonding and interactions between constituents in MOF-5, charge density, charge transfer, and electron localization function (ELF)[40−43] analyses were performed. We have also calculated the optical properties including dielectric function, absorption coefficient, reflectivity, refractive index, optical conductivity, and energy loss function for MOF-5 by using the CASTEP code. The method used for the calculation of optical properties has been proven to be reasonable and compared favorably with corresponding experimental spectra in previous papers from our and other groups.[44−54]

## III. Results and Discussions

**A. Structural Details.** MOF-5, also known as IRMOF-1, is the first member of a series of IRMOFs with oxide-centered $Zn_4O$ tetrahedra as nodes linked by organic molecules and can be synthesized based on the reticular synthesis chemistry proposed by Yaghi et al.[7,55] In MOF-5 the organic linker is 1,4-benzenedicarboxylate (BDC). It should be pointed out that depending on the synthesis procedure and experimental conditions, residual ZnO species in the pores and lattice interpenetration may change the crystal symmetry from cubic to trigonal, and this may affect the physical and chemical properties.[56]

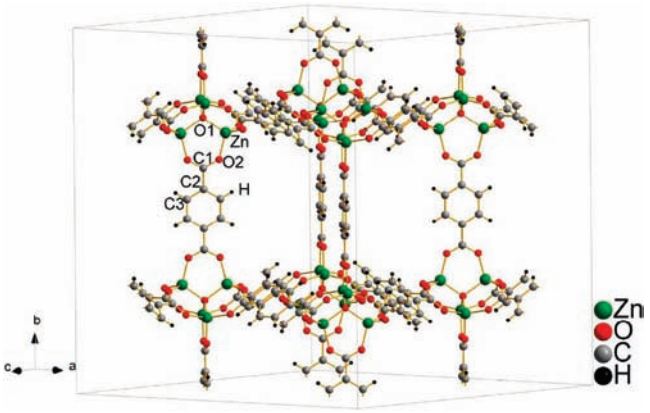


**Figure 1.** Crystal structure of MOF-5 in the cubic $Fm\bar{3}m$ symmetry (no. 225).

MOF-5 can be obtained in highly crystalline form with high specific surface areas in the range 3000−4700 m$^2$/g.[57,58] The conventional cell of its crystal structure has cubic $Fm\bar{3}m$ symmetry (no. 225) with the lattice parameter $a = 25.89$ Å and contains eight formula units of $Zn_4O(BDC)_3$. Its primitive cell includes two nodes and six linker molecules, corresponding to two $Zn_4O(BDC)_3$ formula units. The crystal structure of MOF-5 is illustrated in Figure 1. Different crystallographic sites in MOF-5 includes one type of Zn, two types of O, three types of C, and one type of H occupying 32*f*, 8*c*, 96*k*, 48*g*, 48*g*, 96*k*, and 96*k* Wyckoff positions, respectively.

**B. Structural Optimization of MOF-5 from Total Energy Calculation.** For the structural optimization, the experimentally determined X-ray diffraction structure was used as the starting geometry. The theoretical ground-state structure was obtained from this by full geometry optimization, that is, the atom positions and cell parameters were fully relaxed.

This was achieved by first relaxing the atomic positions globally using the force-minimization technique, by keeping the lattice constant ($a$) and cell volume ($V$) fixed to experimental values. Then the theoretical ground-state volume was determined with optimized atomic positions by varying the cell volume within ±10% of the experimentally determined volume. The calculated total energy as a function of volume was fitted to the so-called equation of state (EOS) to calculate the bulk modulus ($B_0$) and its pressure derivative ($B_0'$). To cross-check the calculated $B_0$ and $B_0'$ values, the E-V data were fitted into three different EOSs, that is, Murnaghan,[59] Birch,[60] and Universal equation of states.[61] The bulk moduli and their pressure derivatives (in parentheses) for MOF-5 are

(40) Becke, A. D.; Edgecombe, K. E. *J. Chem. Phys.* **1990**, *92*, 5397–5403.
(41) Savin, A.; Becke, A. D.; Flad, J.; Nesper, R.; Preuss, H.; von Schnering, H. G. *Angew. Chem., Int. Ed. Engl.* **1991**, *30*, 409–412.
(42) Savin, A.; Jepsen, O.; Flad, J.; Andersen, O. K.; Preuss, H.; von Schnering, H. G. *Angew. Chem., Int. Ed. Engl.* **1992**, *31*, 187–188.
(43) Silvi, B.; Savin, A. *Nature* **1994**, *371*, 683–686.
(44) Ravindran, P.; Delin, A.; Ahuja, R.; Johansson, B.; Auluck, S.; Wills, J. M.; Eriksson, O. *Phys. Rev. B: Condens. Matter* **1997**, *56*, 6851–6861.
(45) Delin, A.; Ravindran, P.; Eriksson, O.; Wills, J. M. *Int. J. Quantum Chem.* **1998**, *69*, 349–358.
(46) Ravindran, P.; Delin, A.; Johansson, B.; Wills, J. M.; Eriksson, O. *Phys. Rev. B* **1999**, *59*, 15680–15693.
(47) Ravindran, P.; Delin, A.; Johansson, B.; Eriksson, O.; Wills, J. M. *Phys. Rev. B* **1999**, *59*, 1776–1785.
(48) Ravindran, P.; Fjellvåg, H.; Kjekshus, A.; Delin, A.; Eriksson, O. *Phys. Rev. B* **2002**, *65*, 0644451–06444519.
(49) Karazhanov, S. Z.; Ravindran, P.; Grossner, U.; Kjekshus, A.; Fjellvåg, H.; Svensson, B. G. *Solid State Commun.* **2006**, *139*, 391–396.
(50) Karazhanov, S. Z.; Ravindran, P.; Vajeeston, P.; Ulyashyn, A.; Finstad, T.; Fjellvåg, H. *Phys. Rev. B* **2006**, *76*, 0751291–07512913.
(51) Brik, M. G. *J. Phys.: Condens. Matter* **2009**, *21*, 485502/1–485502/8.
(52) Chen, J.; Zhao, G.; Sun, Y.; Liu, T. *Solid State Commun.* **2010**, *150*, 897–900.
(53) Xia, Q.; Yi, J.; Li, Y.; Peng, Y.; Wang, H.; Zhou, C. *Solid State Commun.* **2010**, *150*, 605–608.
(54) Cheng, Y. C.; Wu, X. L.; Zhu, J.; Xu, L. L.; Li, S. H.; Chu, P. K. *J. Appl. Phys.* **2008**, *103*, 073707/1–073707/5.
(55) Yaghi, O. M.; O'Keeffe, M.; Ockwig, N. W.; Chae, H. K.; Eddaoudi, M.; Kim, J. *Nature* **2003**, *423*, 705–714.
(56) Hafizovic, J.; Bjørgen, M.; Olsbye, U.; Dietzel, P. D. C.; Bordiga, S.; Prestipino, C.; Lamberti, C.; Lillerud, K. P. *J. Am. Chem. Soc.* **2007**, *129*, 3612–3620.
(57) Wong-Foy, A. G.; Matzger, A. J.; Yaghi, O. M. *J. Am. Chem. Soc.* **2006**, *128*, 3494–3495.
(58) Lin, X.; Jia, J.; Zhao, X.; Thomas, K. M.; Blake, A. J.; Walker, G. S.; Champness, N. R.; Hubberstey, P.; Schröder, M. *Angew. Chem., Int. Ed.* **2006**, *45*, 7358–7364.
(59) Murnaghan, F. D. *Proc. Natl. Acad. Sci. U.S.A.* **1944**, *30*, 244–247.
(60) Birch, F. *Phys. Rev.* **1947**, *71*, 809–824.
(61) Vinet, P.; Rose, J. H.; Ferrante, J.; Smith, J. R. *J. Phys.: Condens. Matter* **1989**, *1*, 1941–1963.

**Table 1.** Optimized Structural Parameters for MOF-5

| property | PBE-GGA | expt[a] |
|---|---|---|
| crystal system | cubic | cubic |
| space group | $Fm\bar{3}m$ (225) | $Fm\bar{3}m$ (225) |
| atoms/cell (fcc) | 106 | 106 |
| $a$ (Å) | 26.0443 | 25.8556 |
| | atomic positions ($x$, $y$, $z$) | |
| atom type | PBE-GGA | expt[a] |
| $Zn_1$ (32$f$) | (0.2936, 0.2936, 0.2936) | (0.2935, 0.2935, 0.2935) |
| $O_1$ (8$c$) | (0.2500, 0.2500, 0.2500) | (0.2500, 0.2500, 0.2500) |
| $O_2$ (96$k$) | (0.2191, 0.7809, 0.3669) | (0.2194, 0.7806, 0.3661) |
| $C_1$ (48$g$) | (0.2500, 0.8890, 0.2500) | (0.2500, 0.8885, 0.2500) |
| $C_2$ (48$g$) | (0.2500, 0.9464, 0.2500) | (0.2500, 0.9461, 0.2500) |
| $C_3$ (96$k$) | (0.7171, 0.2829, 0.4734) | (0.7175, 0.2825, 0.4734) |
| $H_1$ (96$k$) | (0.6918, 0.3082, 0.4520) | (0.6956, 0.3044, 0.4552) |

[a] Experimental data from ref 4.

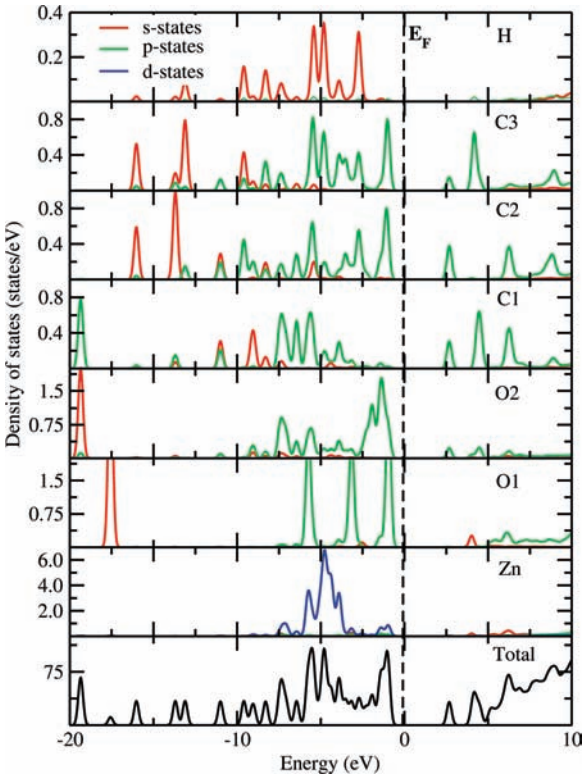


**Figure 2.** Calculated total density of states (TDOS) and partial density of states (PDOS) for MOF-5 in the cubic $Fm\bar{3}m$ symmetry (no. 225).

15.37 GPa (5.06), 15.37 GPa (5.13), and 15.37 GPa (5.17) from the above three EOSs, respectively. This $B_0$ value was found to be comparable with the value of 18.5 GPa previously obtained by VASP calculations by fitting the total energy to a cubic polynomial.[13,16] The calculated bulk moduli are similar to the experimental results and other theoretical data for MOF-5.

The optimized atomic positions and calculated equilibrium lattice parameter along with the corresponding experimental values are listed in Table 1. It can be readily seen that the presently computed results are in excellent agreement with experiment.

**C. Electronic Structure.** The total electronic density of states (TDOS) and partial density of states (PDOS) at the equilibrium volumes of MOF-5 are displayed in Figure 2. It should be pointed out that we have also performed all-electron Dmol3[62,63] calculations to estimate the DOS for MOF-5 to cross-check the DOS obtained from the VASP calculations. The calculated DOS from Dmol3 is almost the same as that from VASP.

The calculated band gap $E_g$ for MOF-5 is 3.5 eV, indicative of semiconductor character, which is in excellent agreement with the experimental value of 3.4−3.5 eV.[14,16] It should be noted that DFT calculated band gaps tend to be generally lower than experimentally determined band gaps.[64] Such an underestimation of the calculated band gaps is an intrinsic feature of the ab initio method and is related to the DFT limitations, namely, not taking into account the discontinuity in the exchange-correlation potential.[65] To overcome this discrepancy, the so-called scissor operator,[66] Δ, can be introduced, which effectively eliminates the difference between the theoretical and experimental gap values by means of a simple rigid shift of the unoccupied conduction band with respect to the valence band. In line with this, for $E_g$ of bulk ZnO, the calculated band gaps are significantly smaller than the experimental values. (LDA = 0.744/0.573 eV; GGA = 0.804/0.641 eV, LDA+U = 1.988/1.486 eV, GW = 2.255/2.100 eV, experimental 3.455/3.300 eV for ZnO-w/-z, respectively).[67] However, for MOF-5 the present DFT calculations unexpectedly gave a band gap value in very good agreement with that obtained from experimental studies.[14,16] It may be of interest to extend this study to other MOFs that are constructed from various organic dicarboxylic acid linkers and the $Zn_4O$ nodes to understand more about the role of these nodes in the electronic structure and optical properties of the materials. Moreover, we are aware that the bond distances of Zn−O are 1.936 to 1.948 Å and 1.974 to 1.983 Å, the angles of O−Zn−O are 107.7° to 111.2° and 108.3° to 110.7° in MOF-5 and bulk ZnO, respectively. Though the bond distances and angles are comparable between MOF-5 and ZnO, significant differences may arise from the isolated nature of the oxide nodes which are expected to act like quantum dots, and also from the perturbation arising from the organic linker BDC.

**D. Chemical Bonding. i. Partial Density of States.** From the PDOS of MOF-5 one can characterize the distribution of various electronic states in the valence band and the conduction band. The d- and s-states Zn and H atoms, respectively, are dominantly contributing to the valence band. Both s- and p-states of C and O atoms also contribute to the VB. The p-states of C1 and C2 are distributed energetically in the same range and thus they can effectively overlap and form very strong covalent bonds. This is consistent with the following analysis of the electron localization function plot, that is, the ELF values between C1 and C2 are higher than that between other C-atoms. Furthermore, valence electrons from both C1 and C2 atoms are also spatially distributed closer to each other to make strong covalent bonds. The s-states of H can

(62) Delley, B. *J. Chem. Phys.* **1990**, *92*, 508–517.
(63) Delley, B. *J. Chem. Phys.* **2000**, *113*, 7756–7764.
(64) Shishkin, M.; Kresse, G. *Phys. Rev. B: Condens. Matter* **2007**, *75*, 235102/1–235102/9.
(65) Perdew, J. P.; Levy, M. *Phys. Rev. Lett.* **1983**, *51*, 1884–1887.
(66) Levine, Z. H.; Allan, D. C. *Phys. Rev. B: Condens. Matter* **1991**, *43*, 4187–4207.
(67) Karazhanov, S. Z.; Ravindran, P.; Kjekshus, A.; Fjellvåg, H.; Grossner, U.; Svensson, B. G. *J. Appl. Phys.* **2006**, *100*, 043709/1–043709/11.

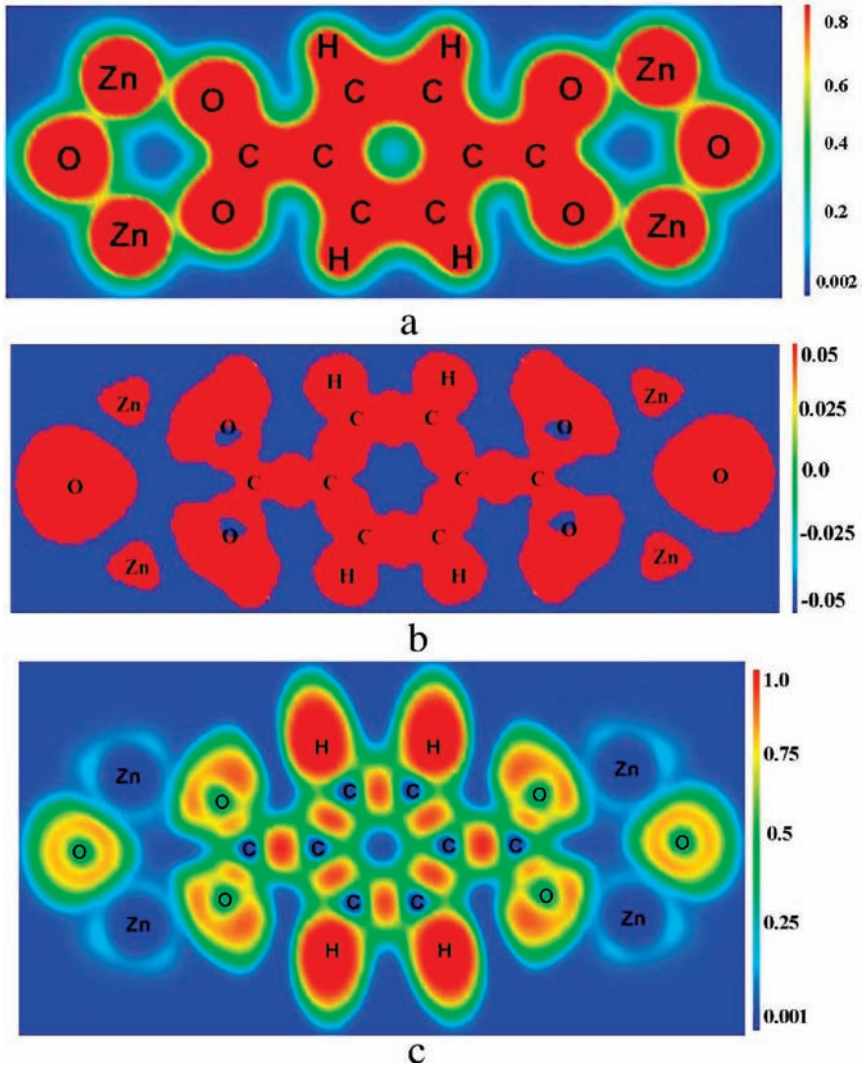


**Figure 3.** Calculated charge density (a), charge transfer (b), and electron localization function (c) plots for MOF-5 in the (110) plane.

overlap with the p-states of C3 in the energy range between −7.5 to −2.5 eV and can form covalent bonds. The p-state of C1 can overlap with that of O2 in the energy range between −7.5 to 0 eV and form a directional bond between them. Although the p-state of C1 is energetically degenerate with that of O1, in the whole valence band, the spatial separation of these two atoms makes no covalent bonding between C1 and O1. The d-state of Zn is well localized, and also the Zn s electrons are transferred to the neighboring atoms, which leads to ionic bonding between Zn and O. This is also consistent with the following analysis of charge density and ELF.

**ii. Charge Density/Transfer, ELF and BOP Analyses.** To further improve the understanding of the bonding interactions, we turn our attention to charge density/transfer, ELF, and bond overlap population (BOP)/Mulliken population analyses. From the illustration in Figure 3a, it is clear that C, H, and O atoms in the organic linker form an $O_2C-C_6H_4-CO_2$ molecule-like structural subunits. As a result, the C−C, C−H, and C−O bonding interactions are dominantly covalent in character. Moreover, there is substantial charge density distributed between C atoms, and between C and H and O atoms in the $O_2C-C_6H_4-CO_2$ subunits. This substantiates the presence of covalent bonding. From Figure 3a, it can be seen that the charges are spherically distributed at the Zn and O sites, which is characteristic for systems having ionic interactions. Additionally, there is no noticeable charge density distributed between Zn and O atoms which clearly demonstrate the presence of ionic bonding. Another convenient and illustrative way to represent and analyze the bonding effects in MOF-5 is to use charge transfer plots. The charge-transfer contour is the difference between the self-consistent electron density in a particular plane, $\rho_{comp}$, and the electron density of the overlapping free atoms in the same lattice, $\rho_{atom}$, that is, $\Delta\rho(r) = \rho_{comp} - \rho_{atom}$. This allows the visualization of how electrons are redistributed in a particular plane compared to free atoms because of the bonding in the compound. From Figure 3b it is clear that electrons are transferred from Zn to O sites. But the charge transfer from Zn is not isotropic as clearly seen from Figure 3a. The anisotropic charge transfer from Zn to the O sites indicates the presence of iono-covalent bonding between Zn and O. But the ionic bonding interaction dominates over the covalent interaction between Zn and O. Furthermore, electron densities from the C, O, and H atoms are transferred to the regions in between these atoms, and the nonspherical electron distribution clearly indicates the presence of strong covalent bonding. From Figure 3c, it can be inferred that the large

**Table 2.** Calculated Mulliken Effective Charge (MEC) and Bond Overlap Populations for MOF-5

| atomic site | MEC (e) | overlap population |
|---|---|---|
| H | +0.29 | 0.89 (C−H) |
| C1 | −0.26 | 0.91 (C−O) |
| C2 | +0.58 | 0.84−1.10 (C−C) |
| C3 | −0.06 | |
| O1 | −1.03 | |
| O2 | −0.63 | |
| Zn | +1.27 | 0.27−0.30 (Zn−O) |

value of ELF at the O site indicates strongly paired electrons with local bosonic character. The negligibly small ELF between Zn and O, and the small value of ELF at the Zn site (partially because of the presence of d electrons) with spherically symmetric distribution indicate that the bonding interaction between Zn and O is dominated by an ionic interaction. The ELF distribution at the O site is not spherically symmetric, and it is polarized toward Zn atoms, indicating the presence of directional bonding between Zn and O. A certain polarized character is found in the ELF distribution at the H sites in MOF-5, indicating the presence of polar covalent bonding. There is a maximum in the ELF between the C atoms and between C and O, indicating the covalent bonds. From the above analyses, one can clearly visualize mixed chemical bonding in MOF-5.

To gain further understanding about the interaction between the constituents, the bond overlap population (BOP) values were calculated on the basis of the Mulliken population analysis.[68] A high BOP value indicates a strong covalent bond, whereas a low BOP value indicates an ionic or a nonbonding interaction. The calculated BOP values for the Zn−O, C−O, C−C, and C−H bonds are displayed in Table 2. A high BOP value indicates a strong covalent bond, while a low BOP value indicates an ionic/nonbonding interaction. From Table 2 it can be seen that the BOP values for the Zn−O bonds in the crystal varies in the range 0.27−0.30, which indicates a dominantly ionic character. Similarly, the calculated BOP value for the C−O bond is 0.91, which is very close to a covalent C−O single bond. The BOP value for C−H is 0.89, indicative of the predominant covalent character. For the C−C bonds, the calculated BOP values vary between 0.84 and 1.10, the latter of which is almost equal to the covalent C−C bond in diamond (1.08), and therefore, the C−C bonds are strong covalent bonds. It should be noted that the order of BOP values is Zn−O < C−H ≈ C−O < C−C. Therefore, the Zn−O bonds in the nodes of MOF-5 have predominant ionic character similar to that present in ZnO, whereas the C−H, C−O, and C−C bonds in the linkers of MOF-5 have covalent interactions such as those in regular organic molecules.

The above discussions demonstrated that analyses based on charge density/transfer, ELF, and bond overlap population (BOP)/Mulliken population analyses give a consistent view of the bonding in MOF-5.

The calculated Mulliken charges are reported in Table 2 for MOF-5. The corresponding Mulliken effective charges (MEC) values for H and Zn are +0.29|e| and +1.27|e|. The C atoms connected to H bear negative charges (−0.26|e|). However, the C atoms bonded to C bear nearly zero charge (−0.06|e|). The C atoms connected to O bear positive charges (+0.58|e|). Finally, the central O that is surrounded by four Zn atoms in the $Zn_4O$ node has a single unit of negative charge (−1.03|e|), which indicates that the four Zn atoms together have transferred a charge corresponding to one electron to the central O. The O atoms in the BDC linker bear negative charges (−0.63|e|) indicating that there is partial electron transfer from Zn to O. From the Mulliken population analysis we can also identify the distribution of electrons in different orbitals. As might be intuitively predicted, for H, the electron is only located at the s orbital; for C and O, electrons are located at both s and p orbitals; and for Zn, electrons are located at s, p, and d orbitals.

**E. Optical Properties.** The studies of the optical properties for MOF-5 are of interest, for example, in view of potential uses of this material in hybrid solar cell applications as an active material or in the buffer layer between the electrodes and the inorganic active materials. Further optical properties studies for MOF-5 are of fundamental importance, since these not only involve the occupied and unoccupied parts of the electronic structure but also carry information about the character of the bands. Moreover, it is also related to the excited states of MOF-5, from which one can gain insight into the excited electronic properties of MOF-5 which may also be important for certain applications. (The moisture sensitivity of MOF-5 may be an obstacle toward many practical uses of this material; there is a risk that certain photocatalytic experimental studies on MOF-5 in reality might be better considered as studies on the photocatalytic properties of decomposition products of MOF-5).

The central quantity of the optical properties is the dielectric function $\varepsilon(\omega)$, which describes the features of linear response of the system to an electromagnetic radiation, which again governs the propagation behavior of radiation in a medium. Here $\varepsilon(\omega)$ is connected with the interaction of photons with electrons. Its imaginary part $\varepsilon_2(\omega)$ can be derived from interband optical transitions by calculating the momentum matrix elements between the occupied and unoccupied wave functions within the selection rules, and its real part $\varepsilon_1(\omega)$ can be derived from $\varepsilon_2(\omega)$ by the Kramer−Kronig relationship.[44] The real part of $\varepsilon(\omega)$ in the limit of zero energy (or infinite wavelength) is equal to the square of the refractive index $n$. All the frequency dependent optical properties, such as refractive index $n(\omega)$, absorption coefficient $\alpha(\omega)$, reflectivity $R(\omega)$, and electron energy-loss spectrum $L(\omega)$ can be deduced from $\varepsilon_1(\omega)$ and $\varepsilon_2(\omega)$.[44]

We have performed CASTEP calculations to estimate the optical properties of MOF-5, and the results from the optical calculations are shown in Figure 4. There are four main peaks in the plot of the imaginary part of the dielectric function, $\varepsilon_2(\omega)$, of MOF-5 (Figure 4a). Three are located at 4.83, 6.07, and 8.21 eV. Another peak is found at somewhat high frequency at 14.61 eV, flanked on each side by two broad peaks at about 12.48 and 18.54 eV. The real part of the dielectric function, $\varepsilon_1(\omega)$, (Figure 4a) allows us to estimate that the value of the refractive index at infinite wavelength is about 1.25. At low frequencies (0−3.5 eV), the imaginary part $\varepsilon_2(\omega)$ is zero below the bandgap, which is consistent with the order of bandgap of MOF-5.

The reflectivity spectrum (Figure 4b) of MOF-5 shows peaks at around 4.49, 5.93, and 8.06 eV. Another peak is

(68) Mulliken, R. S. *J. Chem. Phys.* **1955**, *23*, 1833–1840.

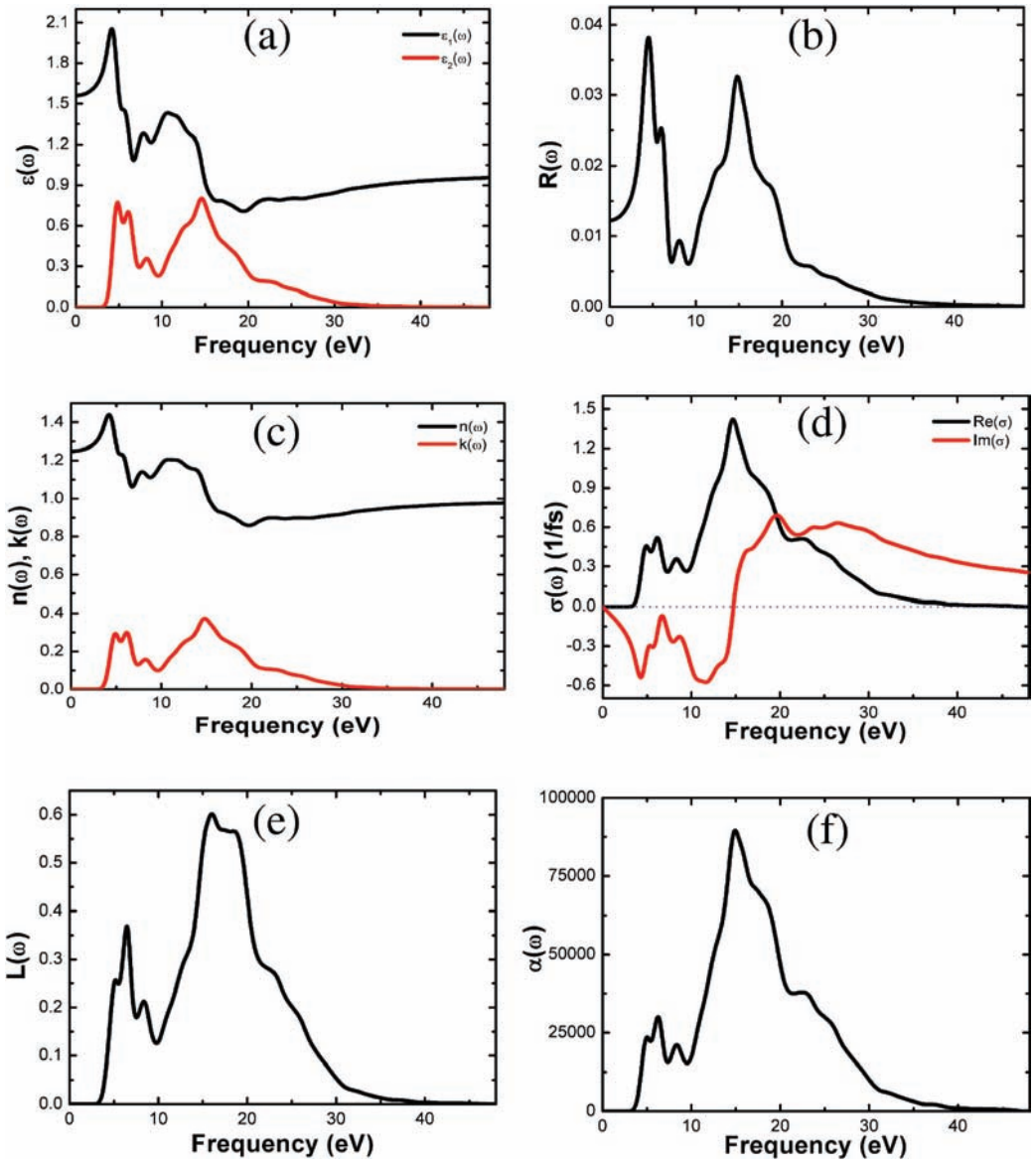


**Figure 4.** Calculated optical properties for MOF-5: (a) dielectric function $\varepsilon(\omega)$, (b) reflectivity $R(\omega)$, (c) refractive index $\mathbf{n}(\omega)$; extinction coefficient $\mathbf{k}(\omega)$, (d) optical conductivity $\sigma(\omega)$, (e) energy loss function $L(\omega)$, f) absorption $\alpha(\omega)$.

located at somewhat higher frequency at 14.81 eV, along with broad shoulders at 12.41 and 18.67 eV. Two sharp peaks are seen in the low frequency region of the reflectivity curve. These two peaks mainly arise from the Zn (3d) → O (2p) interband transitions. This is consistent with the order of bandgap of MOF-5. Another shallow and diffuse peak can be found at around 23.3 eV in the somewhat higher frequency region. The reflectivity index approaches zero when the frequency exceeds 45 eV.

The MOF-5 has a refractive index $n(\omega)$ (Figure 4c) in the range 3.5 to 16.5 eV, and no refractive index in the energy regions lower than 3.5 eV or higher than 16.5 eV. The extinction coefficient $k(\omega)$ (the imaginary part of the complex refractive index) of MOF-5 (Figure 4c) shows three peaks at around 4.97, 6.14, and 8.27 eV, and another peak located at around 14.81 eV can be found in the higher frequency region, together with two broad and diffuse shoulders at around 12.68 and 18.61 eV. Another diffuse and shallow peak can be found at around 22.88 eV.

The optical conductivity $\sigma(\omega)$ plot of MOF-5 is shown in Figure 4d. The real part of the complex conductivity has four sharp peaks at about 4.90, 6.14, 8.27, 14.68, and a rather shallow peak at 22.73 eV. Shoulders are seen at around 18.40 and 25.63 eV; the former is broad, whereas the latter is more narrow and unclear.

The electron energy-loss function $L(\omega)$ (Figure 4e) is an important optical parameter describing the energy loss of a fast electron traversing in a certain material. The peaks in the $L(\omega)$ spectra represent the characteristics associated with the plasma resonance, and the corresponding frequency is the so-called plasma frequency above which the material is a dielectric [$\varepsilon_1(\omega) > 0$] and below which the material behaves like a metallic compound in some sense [$\varepsilon_1(\omega) < 0$]. In addition, the peaks of the $L(\omega)$ spectra overlap the trailing edges in the reflection spectra. The peak of $L(\omega)$ of MOF-5 is at 6.43 eV, which corresponds to the reduction of $R(\omega)$. There are four sharp peaks at about 5.24, 6.43, 8.34, and 15.99 eV, and two additional shoulders are located about 18.61 and 23.09 eV.

The MOF-5 has an absorption band (Figure 4f) from about 3.5 to 40 eV, with four sharp peaks at around 5.03, 6.23, 8.34, 14.96, and a broad peak at about 22.67 eV. Two additional shoulders are located at around 18.46 and 25.76 eV.

**F. Conclusions.** We have presented a detailed investigation on the electronic structure, bonding nature, ground-state properties, and optical properties of MOF-5 using first-principles methods. The following important conclusions are obtained:

(1) The calculations show that MOF-5 is "formed" in the cubic crystal structure; the optimized atomic positions and lattice parameters are in very good agreement with recent experimental and theoretical results.

(2) Electronic charge density, charge transfer, and ELF analyses shed light on the nature of the Zn−O, C−O, C−H, and C−C bonds. The analyses consistently support the notion that the bonding interaction between Zn−O is mainly an ionic interaction, whereas those between C−O, C−H, and C−C are mainly covalent interactions.

(3) Electronic density of states studies show that MOF-5 has a bandgap of about 3.5 eV, resulting in a semiconductor character.

(4) The calculated optical properties of MOF-5 provide useful information for future experimental exploration.

**Acknowledgment.** We gratefully acknowledge the Research Council of Norway for financial support and for the computer time at the Norwegian supercomputer facilities.